VOLUME 37 | NUMBER 6
JUNE 2013

CME
www.wileyhealthlearning.com/jmri

JOURNAL OF MAGNETIC RESONANCE IMAGING

JMRI

Journal of Magnetic Resonance Imaging

AN OFFICIAL JOURNAL OF THE INTERNATIONAL SOCIETY FOR MAGNETIC RESONANCE IN MEDICINE

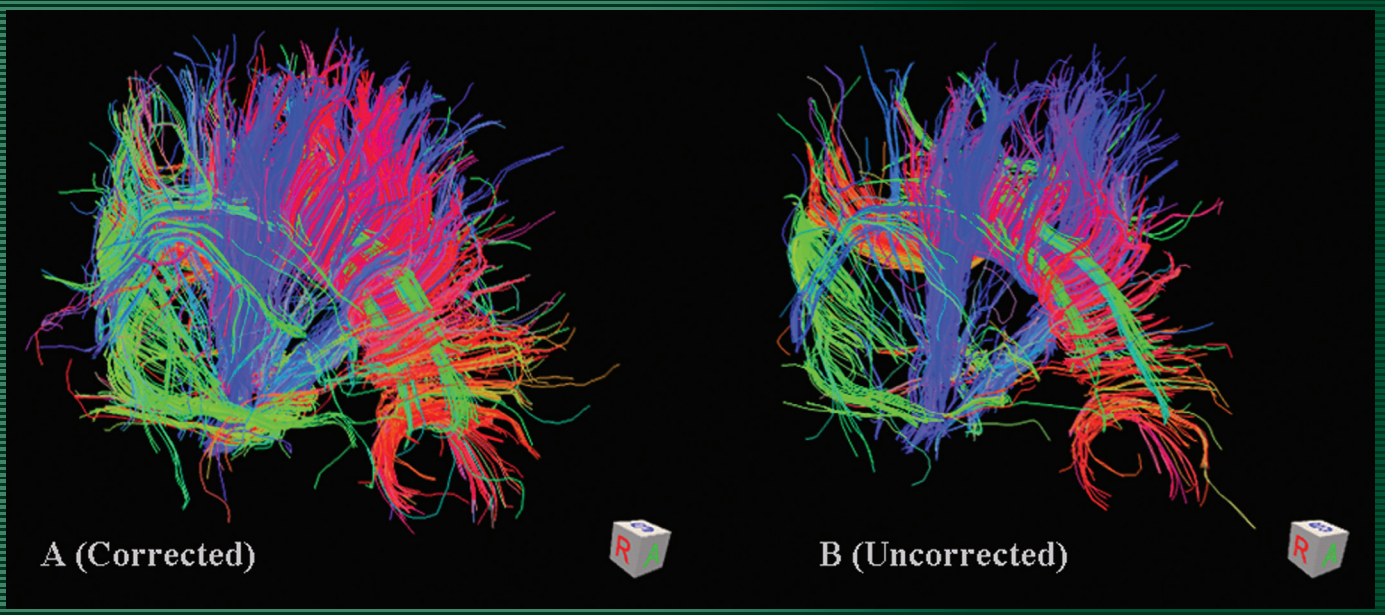

CORRECTION OF EDDY CURRENT DISTORTIONS IN HIGH ANGULAR RESOLUTION DIFFUSION IMAGING
from the article by Zhuang et al (pp 1460-1467)

VOLUME 37 | NUMBER 6 | JUNE 2013 | PAGES 1257–1504

INTERNATIONAL SOCIETY FOR
ISMRM
MAGNETIC RESONANCE IN MEDICINE

Original Research

Correction of Eddy Current Distortions in High Angular Resolution Diffusion Imaging

Jiancheng Zhuang, PhD,* Zhong-Lin Lu, PhD, Christine Bouteiller Vidal, PhD, and Hanna Damasio, MD

Purpose: To correct distortions caused by eddy currents induced by large diffusion gradients during high angular resolution diffusion imaging without any auxiliary reference scans.

Materials and Methods: Image distortion parameters were obtained by image coregistration, performed only between diffusion-weighted images with close diffusion gradient orientations. A linear model that describes distortion parameters (translation, scale, and shear) as a function of diffusion gradient directions was numerically computed to allow individualized distortion correction for every diffusion-weighted image.

Results: The assumptions of the algorithm were successfully verified in a series of experiments on phantom and human scans. Application of the proposed algorithm in high angular resolution diffusion images markedly reduced eddy current distortions when compared to results obtained with previously published methods.

Conclusion: The method can correct eddy current artifacts in the high angular resolution diffusion images, and it avoids the problematic procedure of cross-correlating images with significantly different contrasts resulting from very different gradient orientations or strengths.

Key Words: high angular resolution diffusion imaging; distortions; eddy currents; echo planar imaging
J. Magn. Reson. Imaging 2013;37:1460–1467.

DIFFUSION TENSOR IMAGING (DTI) has become a popular tool to provide information about the intrinsic architecture of white matter in the human brain (1). However, the DTI technology has significant limitations in resolving orientation heterogeneity within single voxels due to the constraints of tensor models. As an obstacle for efforts to construct white matter pathways from diffusion magnetic resonance imaging (MRI) data, this limitation has prompted the development of diffusion imaging methods capable of resolving intravoxel fiber crossings, such as HARDI (high angular resolution diffusion imaging) (2). Among HARDI techniques, diffusion spectrum imaging (DSI) employs the Fourier relationship between the diffusion signal and the function of diffusion wave vector q (3), and q-ball imaging (QBI) uses Funk–Radon transform to process the HARDI signal (4).

However, because most of the HARDI techniques require high to ultrahigh diffusion sensitizing gradients (b $>$4000 s/mm^2), the capability of HARDI to provide valid and reliable information about tissue structures can be affected adversely by eddy current artifacts. In echo planar images, usually used to acquire diffusion-weighted images (DWI), eddy currents produce significant distortions in the phase-encoding direction because of the relatively low bandwidth in that direction and the large changes in diffusion gradients during HARDI scanning. Image distortions from eddy currents blur the interface of gray and white matter tissues, cause misregistration between individual diffusion-weighted images, produce erroneous calculations of diffusion signals, and spoil the detected high angle-resolution characteristics of diffusion at each voxel.

Eddy current distortions can be reduced effectively in one of three ways: first, by selecting an appropriate pulse sequence (such as a dual spin-echo sequence) (5,6) or gradient waveforms (such as bipolar gradients) (7); second, by correcting *k*-space data, such as calibration of eddy current artifacts in *k*-space (8–10); third, by postacquisition image processing that registers DWIs to the reference images. This third approach, based on postprocessing algorithms, is appealing because of its relative ease and accessibility. One widely used postprocessing algorithm, iterative cross-correlation (ICC) (11), estimates distortions in DW images by cross-correlating them with an undistorted baseline image in terms of *scaling, shear*, and *translation* along the phase-encoding direction. The estimated distortion parameters are then used to correct all distorted images (11–14).

One serious limitation of the original ICC algorithm (11), however, is its inability to correct image distortions at high b-values. The contrasts of cerebrospinal fluid (CSF), gray matter, and white matter in images

Dana and David Dornsife Cognitive Neuroscience Imaging Center, University of Southern California, Los Angeles, California, USA.
*Address reprint requests to: J.Z., 3620 South McClintock Ave., SGM 501, Los Angeles, CA 90089. E-mail: jc.zhuang@gmail.com
Received January 31, 2012; Accepted October 1, 2012.
DOI 10.1002/jmri.23929
View this article online at wileyonlinelibrary.com.

acquired with no diffusion weighting differ greatly from the contrasts found in images acquired with high (b-value) diffusion weighting. The contrast differences lead to unreliable registration of the two types of images, which in turn interferes with eddy current distortion corrections. This problem is more serious in most q-space diffusion images for which high or ultrahigh b-values are commonly used (2–4).

Various methods have been proposed to more accurately estimate effects of eddy current distortions. Some investigators proposed a method of extrapolating distortion parameters from low to high b-value images (11). Others employed the ICC algorithm with reference to CSF-suppressed images (such as FLAIR) to minimize the major source of contrast change in images acquired with different b-values (15). DWIs of a water phantom have also been used to measure distortion parameters directly, and these parameters can then be used to calibrate the ICC of brain images (13). Although these procedures extend the possibility to use the ICC algorithm with b-values as high as 2000 $s{\cdot}mm^{-2}$, they require acquisition of additional images that prolongs scanning times, which is not always desirable.

Two recent approaches use only DWIs to estimate relative distortions. One approach, coregistration of pairs of DW images with exactly the reversed diffusion gradients followed by corrections of the distortions using ICC, will double the acquisition time (14); the other, applying the known gradient strength and direction to model the absolute distortions only between DW images, may involve inaccurate image coregistration, especially at ultrahigh diffusion gradient strength, due to image contrast differences resulting from changes of diffusion gradient directions (16).

Here we describe a new algorithm to detect eddy current distortions by modeling the distortion with the known x, y, and z components of diffusion gradients exclusively from DW images with close diffusion gradient directions. The algorithm was validated in experimental data. Finally, we demonstrate its successful application to correct distortions in DWIs of the human brain.

MATERIALS AND METHODS

Theory

Diffusion-sensitizing gradients consist of components along each of the x, y, and z axes. The eddy currents induced by a change in a single gradient component, the x gradient, for example, can be distributed along the x, y, and z axes. Such eddy currents produce residual gradient fields in the frequency encoding, phase encoding, and slice-selection directions. These residual gradients in turn cause shearing, scaling, and translational distortions, all visible along the phase-encoding direction of echo-planar images (EPIs) (11). Assuming that the interaction between these three components of gradient fields is negligible (14), the total eddy current distortion will be equal to the linear sum of the distortion induced by the x, y, and z gradients (16).

Accordingly, the x, y, and z components of the i-th diffusion gradient $\mathbf{G}_i = (G_{ix}, G_{iy}, G_{iz})$ will produce a corresponding image translation distortion $\mathbf{G}_i\mathbf{T} = G_{ix}T_x+G_{iy}T_y+G_{iz}T_z$, where $\mathbf{T} = (T_x, T_y, T_z)$ is the translation along the phase-encoding direction induced by the corresponding unit changes in the x, y, and z gradients. The resulting distortion in translation D_{ti} from the alignment between the images of the i-th diffusion gradient direction and the j-th (reference) gradient direction can be calculated for $i \neq$ j as:

$$D_{ti} = (G_{ix}T_x + G_{iy}T_y + G_{iz}T_z) - (G_{jx}T_x + G_{jy}T_y + G_{jz}T_z),$$

or

$$\boldsymbol{G}' \cdot \boldsymbol{T} = \boldsymbol{D}_t,$$

where the rows of matrix $\mathbf{G}'$ are formed by the differences (G_{ix}–$G_{\mathrm{j}x}$, G_{iy}–$G_{\mathrm{j}y}$, G_{iz}-$G_{\mathrm{j}z}$) for the i-th diffusion gradient, and $\mathbf{D}_t$ is the distortion vector of image translation that is measured by the registration between the reference image and the images from other diffusion gradients. The three unknown elements of vector $\mathbf{T}$ can be calculated as:

$$\mathbf{T} = (\mathbf{G}'^{T} \cdot \mathbf{G}')^{-1} \cdot \mathbf{G}'^{T} \cdot \mathbf{D}_t, \qquad [1]$$

where the superscripts "T" and "–1" denote matrix transposition and inversion, respectively.

Similarly, a vector $\mathbf{S}$ of the shear distortion induced by a unit change of the x, y, and z components of the gradient can be calculated using the following equation:

$$\mathbf{S} = (\mathbf{G}'^{T} \cdot \mathbf{G}')^{-1} \cdot \mathbf{G}'^{T} \cdot \mathbf{D}_s, \qquad [2]$$

where $\boldsymbol{D}_{\boldsymbol{s}}$ is the vector for shearing, which is measured by coregistering the image from the i-th diffusion gradient with that from the j-th diffusion gradient.

Scaling (or magnification) distortion D_{mi}, measured by comparing the image from the i-th diffusion gradient and the image from the j-th (reference) diffusion gradient, can also be calculated for $i \neq$ j as:

$$D_{mi} = \frac{1 + G_{ix}M_x + G_{iy}M_y + G_{iz}M_z}{1 + G_{jx}M_x + G_{jy}M_y + G_{jz}M_z}, \qquad [3]$$

where M_x, M_y, and M_z are the unknown components of scaling induced by unit changes in the x, y, and z gradient components, respectively.

Therefore the following can be derived:

$$\mathbf{G}'' \cdot \mathbf{M} = \mathbf{D}'_m, \qquad [4]$$

where the matrix $\mathbf{G}''$ is formed as (G_{ix}–$D_{mi}G_{\mathrm{j}x}$, G_{iy}–$D_{mi}G_{\mathrm{j}y}$, G_{iz}–$D_{mi}G_{\mathrm{j}z}$) and $D'_{mi} = D_{mi} - 1$ for $i \neq j$. The vector $\mathbf{M} = (M_x, M_y, M_z)$ can thus be obtained from:

$$\mathbf{M} = (\mathbf{G}''^{T} \cdot \mathbf{G}'')^{-1} \cdot \mathbf{G}''^{T} \cdot \mathbf{D}'_m. \qquad [5]$$

Equations 1, 2, and 5 are basically least-squares estimates for $\mathbf{T}$, $\mathbf{S}$, and $\mathbf{M}$. Given the model parameters for the distortions $\mathbf{T}$, $\mathbf{S}$, and $\mathbf{M}$, we can determine the total distortions for the i-th diffusion gradient in

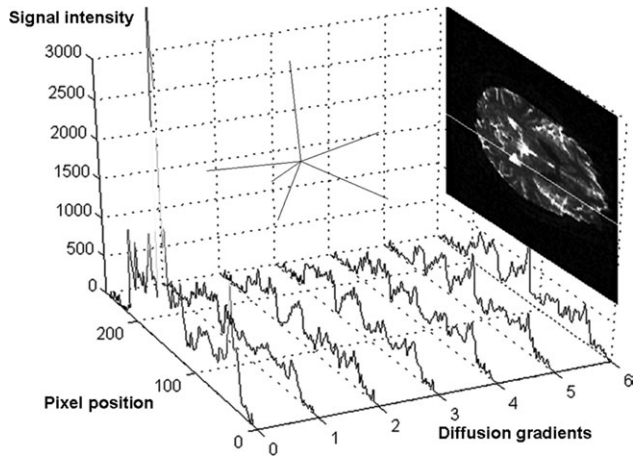

Figure 1. DW image signal intensity changes with diffusion gradient directions (at b = 3000 s/mm^2). On the x axis, 0–6 represents the nondiffusion-weighted and six different diffusion gradient directions (displayed as lines on the background). The y axis represents the pixel position at the 55th column highlighted as a white line in the nondiffusion-weighted image on the right side. The z axis represents MR signal intensity.

relation to the undistorted, non-DW images using the dot products of $\mathbf{G_i}\cdot\mathbf{T}$, $\mathbf{G_i}\cdot\mathbf{S}$, and $\mathbf{G_i}\cdot\mathbf{M}$. Thereafter, image distortions can be corrected by reverse application of these parameters to the distorted DW images, and the DW images will be automatically registered to the non-DW images.

As just seen, the accuracy of the estimation of **T**, **S**, and **M** depends on the coregistration between the images obtained with the *i*-th and *j*-th diffusion gradient directions. If the orientations of the *i*-th and *j*-th diffusion gradient vectors are very different, the contrast difference between the images acquired with these diffusion gradients will be large (Fig. 1). Thus, the coregistration needed to derive the distortion parameters **T**, **S**, and **M** can be inaccurate. On the other hand, if the orientations of the diffusion gradient vectors are similar, the contrast difference between the corresponding DW images is small, and the coregistration might be good enough to obtain the correct distortion parameters.

Material

Five young adults with no history of neurological disease (three males and two females) were scanned on a Siemens 3T Trio Tim MRI system (Siemens Healthcare, Erlangen, Germany). HARDI data were acquired using a single-shot spin-echo echo planar sequence with the following parameters: relaxation time (TR) = 10,000 msec, echo time (TE) = 110 msec, 128 diffusion gradient directions, 51 axial slices for whole-brain coverage, field of view (FOV) = 240 × 240 mm^2, and matrix = 96 × 96, 2.5 mm in-plane resolution and 2.5 mm slice thickness. Three of the subjects were scanned with a single 5000 s/mm^2 b-value. The two remaining subjects were scanned using a range of b-values: 1000 s/mm^2, 3000 s/mm^2, 5000 s/mm^2, 7000 s/mm^2, and 9000 s/mm^2. We also scanned a phantom with the exact same parameters and the same range of b-values used for the latter two subjects. All subjects gave written informed consent according to national guidelines and those of the Institutional Review Board at the university.

Algorithm Implementation

The ICC algorithm was used to coregister between DW images and obtain distortion vectors $\mathbf{D_t}$, $\mathbf{D_s}$, and $\mathbf{D_m}$. It iteratively compared the scaling, shearing, and translation of each phase-encoding column (the *y*-axis in our case) on the distorted image in relation to the reference image (11,14). In each slice we assumed one parameter for shearing, one for translation, and one for scaling. The 1D scaling transformation along y is achieved by linear interpolation, and the shearing can be viewed as a series of progressively larger translations at each phase-encoding column. The normalized cross-correlation function between the new adjusted image and reference image can be calculated. The iterations were performed by varying the parameters of translation in increments of 0.25 pixels, the shearing in increments of 0.005 pixel/column, and scaling factor in increments of 0.005. The fine incremental step was selected as described in previous studies (13,14). The position of the maximum index in the iterative cross-correlation array indicated the optimal

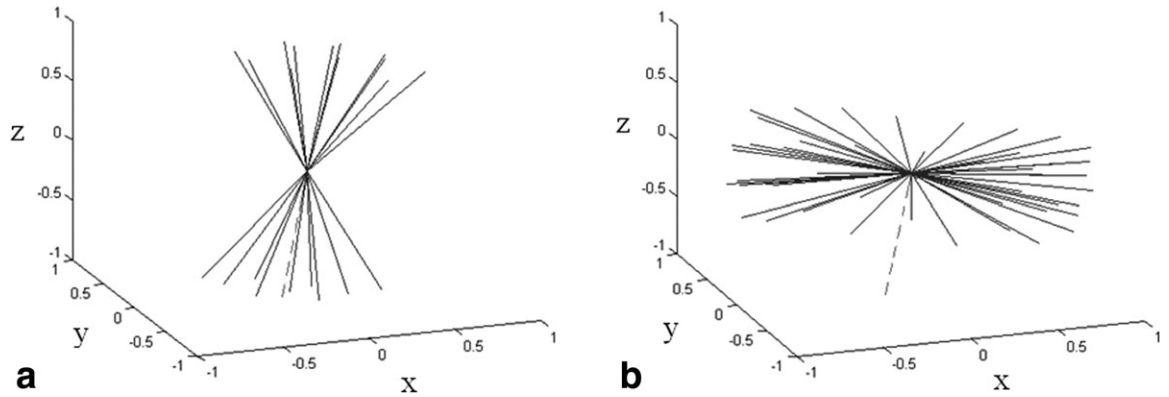

Figure 2. Examples of the close (**a**) and far-away (**b**) diffusion gradient directions, relative to the direction of diffusion gradient in the reference DW image (represented by the dashed line in the figure).

translation, scaling, and shearing parameters required for the registration of two images.

We selected six sets of DW images for coregistration and model fitting from the 128 DWIs in our study. In each set, one image is used as the reference image and the other 15 used for coregistration have the closest spatial directions of diffusion sensitizing gradients with the reference image (Fig. 2). The criteria for selecting the sets of images were: the diffusion gradient directions of the reference images were randomly selected with one exclusion criterion, that the angle difference between any pair of the gradient vectors of the six reference images had to be between 30° and 150° (the maximum possible angle is 180°). Within each set of DW images, the angle difference of the diffusion gradient vectors between the DW images to be coregistered and the reference image had to be always less than 30° or more than 150°.

Therefore, coregistration is only performed within each set of DW images with close diffusion gradient directions. The distortion components of shearing, scale, and translation were calculated for each set of gradient directions using Eqs. [1], [2], and [5]. The parameters **T**, **S**, and **M** calculated from these six sets were averaged into one set of parameters (shearing, scale, and translation), and subsequently used to correct the corresponding distortions for all 128 gradient directions. Our algorithm was implemented in MatLab 7.0 (MathWorks, Natick, MA), requiring about 10 minutes to correct one dataset on a 3.0 GHz Intel Xeon personal computer. Matrix inversions were calculated by MatLab's implementation of LAPACK (Linear Algebra PACKage) (17).

Test of Coregistration Between DW Images and Validation of Model Fitting of Eddy Current Distortions

To test the validity of the coregistration algorithm between images with large diffusion gradient differences, we performed the ICC calculation on the two human datasets with varying diffusion gradient directions and strengths (b-values as 1000 s/mm^2, 3000 s/mm^2, 5000 s/mm^2, 7000 s/mm^2, and 9000 s/mm^2). One reference DW image was randomly selected on each dataset. The ICC coefficients were obtained between images without any prior coregistration. The DW images of the human subjects were visually inspected for head movement. If a head motion was detected or the coregistration between the image and reference image was too poor, the corresponding image was discarded.

Another validation of our proposed algorithm was conducted using both the phantom and human data. Coregistration was only performed between the 16 images that had the closest diffusion gradient orientations. The distortion components of shearing, scale, and translation were calculated for each set of these 16 gradient directions using Eqs. [1], [2], and [5]. The parameters obtained from these six sets were compared and plotted together. For the purpose of comparison, six sets of 16 DW images with very different or far-away diffusion gradients (angle difference of gradient orientations is between 30° and 150°) were used to calculate distortion parameters as well (Fig. 2). Because the phantom differs minimally in contrast between different DW images, the results obtained on the phantom data serve as a reliable benchmark for the evaluation of the algorithm.

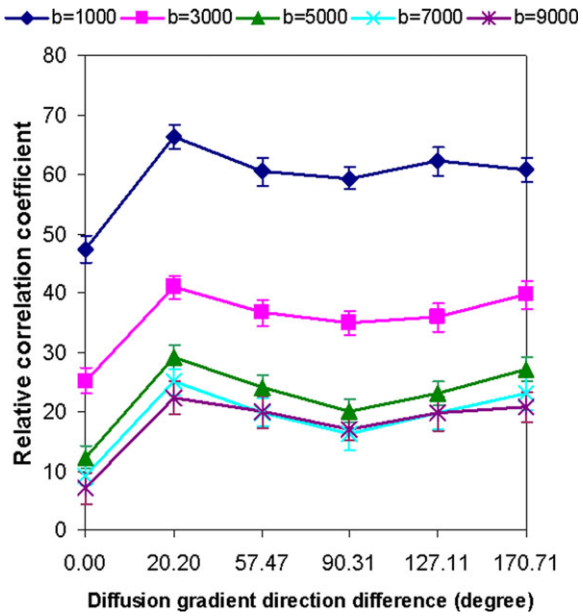

Figure 3. Correlation coefficients of ICC between DW images of human subjects depend on the spatial angle difference of diffusion gradients and gradient strength (b-values in units of s/mm^2). The cross-correlation was performed between one reference DW image (randomly selected as the 51st images in the 128 diffusion directions) and other six images with diffusion gradient angle difference listed on x axis. The "0" gradient direction on the x axis represents the correlation of the reference DW image with a nondiffusion-weighted image.

Correction of Eddy Current Distortions on Q-ball Images From the Human Brain

Q-ball reconstruction was implemented using FRT (Funk–Radon transform) (4) on a pixel-by-pixel basis from the DW data obtained in the three subjects scanned with only a single b-value of 5000 s/mm^2. The diffusion ODF (Orientation Distribution Function) was reconstructed for each voxel using the matrix FRT, a linear matrix formulation based on spherical radial basis function interpolation. Each ODF was then smoothed and divided by the (maximum-minimum) value for normalization to emphasize the orientation structure of the ODF. The Q-ball Imaging (QBI) data were further processed using Trackvis (18) for fiber tracking (19).

We compared the images corrected by our proposed algorithm with the corrected images using the original ICC method (11) and with uncorrected images. Using an index from Bastin and Armitage (13), we quantified improvement in the resulting DW images by counting the number of pixels in which any of the three diffusion eigenvalues was negative in all image slices. A larger value of this index indicates DW images of poorer quality. Such calculated index was compared

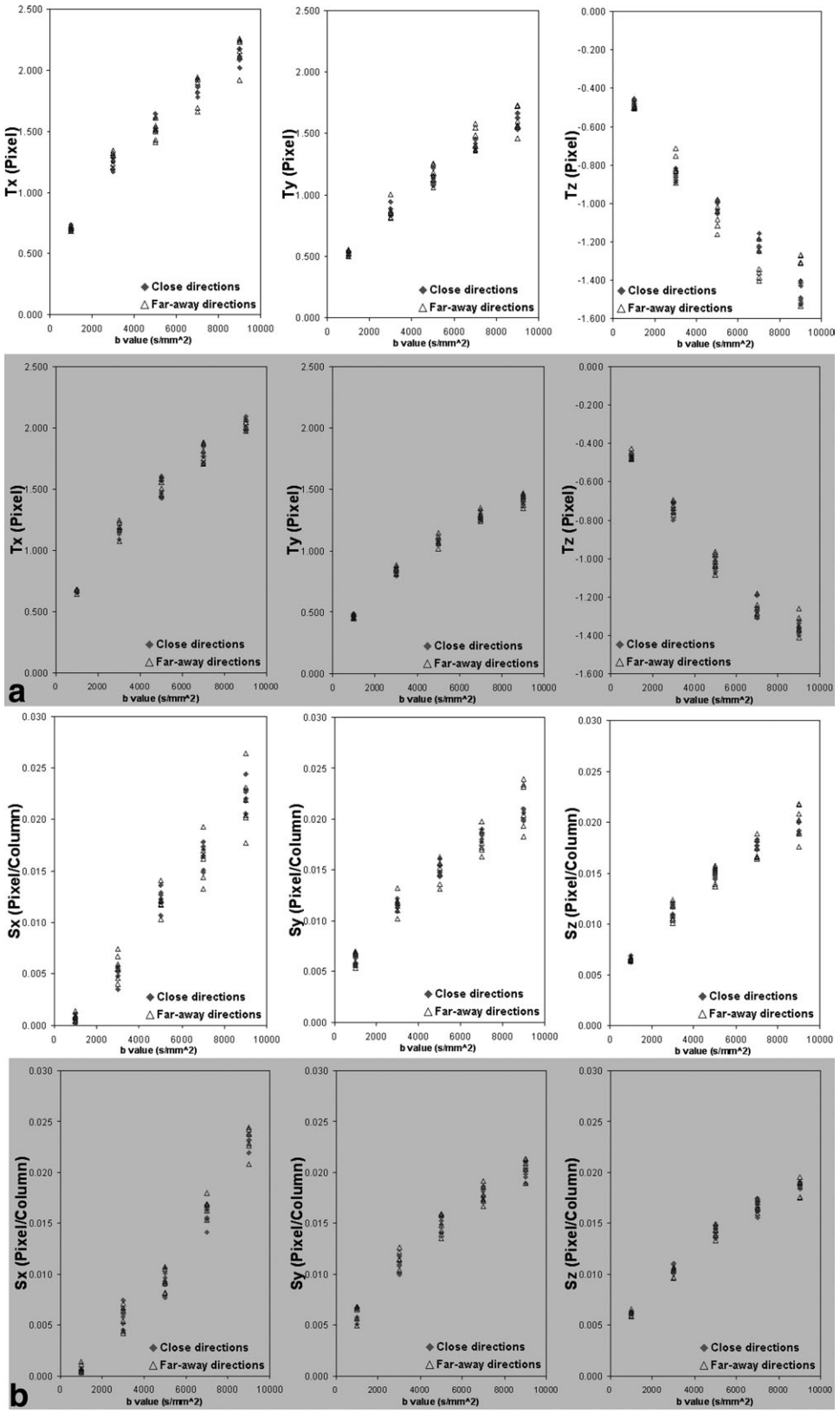

Figure 4. All resulting distortion components (**T, S**, and **M** in Eqs. [1–5]) from model fitting on the human data (with white background) and the phantom data (with gray background), using six sets of close (diamond marker) or far-away (triangle marker) diffusion gradients, as functions of the b-value.

among the corrected DW images using our algorithm, the corrected images using the original ICC method, and the uncorrected DW images. Furthermore, we compared the fiber length detected from corrected and uncorrected images. Fiber tracking of poor DWI data can not resolve fiber-crossing within voxels without

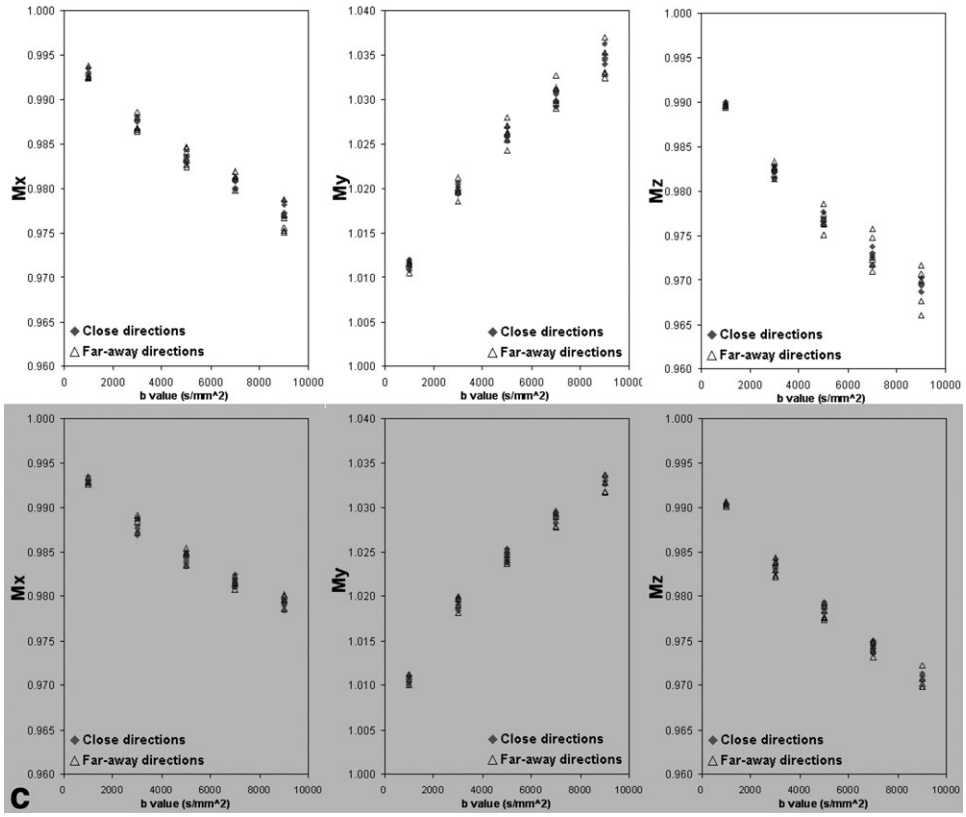

Figure 4. (Continued)

errors, rendering the tracks incomplete. Thus, the resulting fiber lengths from uncorrected images are shorter than those obtained in corrected images. In other words, a shorter average fiber length may reflect poorer quality of fiber tracking. We compared the average fiber length obtained in corrected DW images using our algorithm, with those obtained from corrected images using the original ICC method and uncorrected DW images.

RESULTS

The ICC algorithm did not give high correlation coefficients in coregistering the same slices with far-away diffusion gradient directions when the diffusion weight was higher than 3000 s/mm^2 (Fig. 3). But when the diffusion gradient directions were close enough, the ICC algorithm did provide reliable coregistration at the same diffusion weight. When diffusion weight was lower than 3000 s/mm^2, the ICC calculation provided good coregistration on the same slices between different gradient directions, independent of gradient orientation differences. A further test indicated that the results of correlation coefficients were similar to those obtained with a different reference DW image.

We calculated the values of eddy current distortions, in the phantom experiment, in relation to the DW images with close diffusion gradient directions using our modeling method. The results were compared to those of DW images with large differences in diffusion gradient directions. The results from the two sets of calculations were in close agreement across all gradient directions (Fig. 4). The distortion parameters obtained from six sets of far-away diffusion gradients were also close to each other under the circumstance that the contrast of DW images on the phantom differs minimally between these different diffusion gradients, further supporting the validity and accuracy of the proposed algorithm. On the human data, the distortion components calculated from six sets of images with large diffusion gradient differences were not consistent. However, the distortion components calculated from six sets of close diffusion gradients were relatively consistent (Fig. 4). In our results, each T, S, or M was calculated from the normalized gradient tables without considering the absolute b-value. Among different b-values, the resulting parameters may not be identical even after taking the b-value into account, because different separation times and durations of diffusion gradients were used to achieve the different b-values on the scanner.

In the QBI analysis on human data, tractography performed on images corrected by our method shows fiber tracks with smoother contours and higher number of tracked fibers than the fiber maps constructed without correction (Fig. 5a,b). The average length of tracked fibers increased significantly ($P < 0.0001$) after applying our correction (Table 1). Bastin and Armitage's index (13) also decreased significantly ($P < 0.0001$) after applying our correction method (Table 2). In contrast, the correction using the original Haselgrove's method did not result in a statistically significant improvement

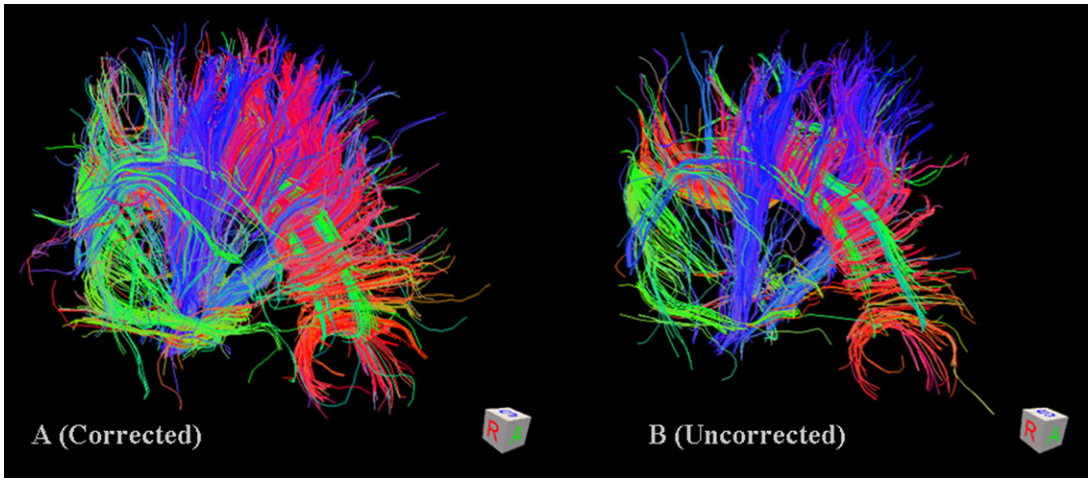

Figure 5. Representative fiber tracking results constructed from the QBI data of a human brain, with and without the eddy current correction proposed in this study. The colors of the fibers indicate the major directions of fibers. The proposed algorithm increased both the number and average length of the tracked fibers (see Table 1 for details).

(Tables 1, 2). This result also underscores the effectiveness of the proposed algorithm.

Our results show that the contrasts of DW images vary with the strength and direction of diffusion gradients, especially when high gradient strength is applied (Figs. 1, 3). When images acquired with similarly oriented diffusion gradients are coregistered, the detected components of translation, shearing, and scaling in eddy current distortions depend linearly on the corresponding diffusion gradient vector. Moreover, this dependence can be exploited to correct eddy current distortions by using the known strength and direction of diffusion gradients applied in DWI acquisition.

DISCUSSION

Our algorithm needs to estimate 3 (distortions) × 3 (components of diffusion gradients) = 9 unknown parameters. Every pair of DW images gives 3 distortion parameters of shear, scale, and translation. To solve the equations for these 9 unknown variables, we need 3 images (to be registered) + 1 image (as reference) = 4 diffusion gradient directions. Thus, for our algorithm to be effective each set of DW images to be coregistered requires at least four diffusion gradient directions, and these four diffusion gradient directions must be spatially close (angle differences less than 30° or more than 150°). It is difficult to find such close gradient directions if only a small number of diffusion gradients are applied, such as in conventional DTI scans. Fortunately, most conventional DTI scans use b-values lower than 2000 s/mm^2, so that some of the existing methods (16) are sufficient to appropriately correct eddy current distortions in those cases. With more gradient directions, as regularly applied in HARDI studies, diffusion gradients with closer orientations are available and higher accuracy

Table 1
Mean Fiber Length Obtained From Uncorrected Images, Images Corrected by Haselgrove's Algorithm and Images Corrected by Our Algorithm on Human Brains

Method	Mean (mm)	SD
Uncorrected	57.4	(17.6)
Haselgrove's algorithm	59.3	(16.3)
Proposed algorithm	68.9	(22.4)

Comparison	*t* value	*P*-value
Haselgrove's algorithm vs. uncorrected	3.3	(>0.001)
Proposed algorithm vs. uncorrected	18.5	(<0.0001)
Proposed algorithm vs. Haselgrove's	15.7	(<0.0001)

The table indicates the fiber length averages (Mean) from all detected fibers, standard deviations (SD), and *t*-tests (Comparison) between the numbers of different methods (described in Methods about Q-ball imaging of human subjects).

Table 2
Comparisons of Bastin and Armitage's Index (13) Among the Uncorrected Images, Images Corrected by Original Haselgrove's Algorithm, and Images Corrected by the Proposed Algorithm

Method	Mean	SD
Uncorrected	75.5	(24..3)
Haselgrove's algorithm	73.5	(21.6)
Proposed algorithm	61.3	(20.4)

Comparison	*t* value	*P*-value
Haselgrove's algorithm vs. uncorrected	2.72	(>0.001)
Proposed algorithm vs. uncorrected	20.5	(<0.0001)
Proposed algorithm vs. Haselgrove's	19.3	(<0.0001)

The table indicates the slice averages (Mean) from all slices, standard deviations (SD), and *t*-tests (Comparison) for the number of pixels containing negative eigenvalues (described in Methods about Q-ball imaging of human subjects).

can be achieved in solving the nine parameters necessary for our method. The b-values used in most HARDI studies are often higher than 2000 s/mm^2, which makes our algorithm more desirable for the correction of eddy current distortions in HARDI than other methods. In this study, selecting the six sets of 16 DW images is required to minimize the estimation error in the algorithm with the maximum possible close gradient orientations in each set.

There have been two previous attempts to model geometric distortions based on gradient directions. One of them calibrated eddy current distortions in each of three orthogonal diffusion gradients in a phantom scan, and subsequently applied the results to ascertain the distortions in DW images acquired with arbitrary gradient amplitudes and directions in a human scan (13). However, eddy current distortions can depend on the detailed experimental conditions and scan parameters for each scan, such as RF coil, TE, slice orientation, and isocenter offset. This dependence is difficult to calibrate in advance, but can be modeled on a scan-by-scan basis using our proposed algorithm. The other approach used a mathematical framework to model geometric distortions based on slice position and gradient direction (20). Both of these approaches coregister DW images without considering whether the orientation of their diffusion gradients are close or far away, which in reality is only applicable to some diffusion imaging data obtained at low diffusion gradient strengths.

In this study we only tested our algorithm for the Q-ball imaging method. The algorithm is also suitable for other regular HARDI methods, such as DSI, when the diffusion gradient strength (b-value) does not vary excessively. If gradient strength changes dramatically with each diffusion gradient vector, such as in some multiple wave-vector diffusion imaging methods, the assumption in our algorithm will need further verification.

Another common artifact in HARDI data is due to head movement. The difficulty to correct head movement artifact in HARDI is similar to that for eddy current correction, especially in terms of coregistering between DW images. The effects of these two artifacts can get mixed together, making postprocessing more difficult and confounding. It is difficult to separate the effects from head motion and eddy current in DW images. But head movements are random and independent of diffusion gradients. Therefore, the results from our Eqs. [1–5], which have high correlation with the diffusion gradients, have already discounted the effects of head movements. Furthermore, estimation errors from head motion were reduced by averaging the results from six subsets of DW images in our algorithm. In future work we will continue our effort to completely separate the effects of eddy currents and head motion in HARDI data postprocessing.

The proposed approach implicitly assumes that the time constants of significant eddy currents are long relative to the EPI readout to allow simple decomposition of eddy current distortions into translation, shear, and scale. This may not be true if a different spectrometer or a different sequence is used. The linearity assumption of the model should therefore be verified after any such change is made, as well as after adjustment of the time constants in the eddy current compensation circuits.

In conclusion, the proposed method for eddy current distortion correction is both accurate and feasible in real-world settings. The method not only circumvents the difficulties of prior published correction algorithms that are associated with large contrast differences across high b-value DW and non-DW images, but also eliminates the requirement to acquire additional images specifically meant for distortion correction.

REFERENCES

1. Basser PJ, Mattiello J, LeBihan D. Estimation of the effective self-diffusion tensor from the NMR spin echo. J Magn Reson B 1994;103:247–254.
2. Tuch DS, Reese TG, Wiegell MR, Makris N, Belliveau JW, Wedeen VJ. High angular resolution diffusion imaging reveals intravoxel white matter fiber heterogeneity. Magn Reson Med 2002;48:577–582.
3. Wedeen VJ, Hagmann P, Tseng WI, Reese TG, Weisskoff RM. Mapping complex tissue architecture with diffusion spectrum magnetic resonance imaging, Magn Reson Med 2005;54:1377–1386.
4. Tuch DS. Q-Ball imaging. Magn Reson Med 2004;52:1358–1372.
5. Wider G, Dotsch V, Wuthrich K. Self-compensating pulsed magnetic-field. Gradients for short recovery times. J Magn Reson A 1994;108:255–258.
6. Reese TG, Heid O, Weisskoff RM, Wedeen VJ. Reduction of eddy current-induced distortion in diffusion MRI using a twice-refocused spin echo. Magn Reson Med 2003;49:177–182.
7. Alexander AL, Tsuruda JS, Parker DL. Elimination of eddy current artifacts in diffusion-weighted echo-planar images: the use of bipolar gradients. Magn Reson Med 1997;38:1016–1021.
8. Jezzard P, Barnett AS, Pierpaoli C. Characterization of and correction for eddy current artifacts in echo planar diffusion imaging. Magn Reson Med 1998;39:801–812.
9. Calamante F, Porter DA, Gadian DG, Connelly A. Correction for eddy current induced B0 shifts in diffusion-weighted echo-planar imaging. Magn Reson Med 1999;41:95–102.
10. Papadakis NG, Smponias T, Berwick J, Mayhew JEW. K-space correction of eddy-current-induced distortions in diffusion-weighted echo-planar imaging. Magn Reson Med 2005;53:1103–1111.
11. Haselgrove JC, Moore JR. Correction for distortion of echo-planar images used to calculate the apparent diffusion coefficient. Magn Reson Med 1996;36:960–964.
12. Horsfield MA. Mapping eddy current induced fields for the correction of diffusion-weighted echo planar images. Magn Reson Imaging 1999;17:1335–1345.
13. Bastin ME, Armitage PA. On the use of water phantom images to calibrate and correct eddy current induced artefacts in MR diffusion tensor imaging. Magn Reson Imaging 2000;18:681–687.
14. Bodammer N, Kaufmann J, Kanowski M, Tempelmann C. Eddy current correction in diffusion-weighted imaging using pairs of images acquired with opposite diffusion gradient polarity. Magn Reson Med 2004;51:188–193.
15. Bastin ME. On the use of the FLAIR technique to improve the correction of eddy current induced artefacts in MR diffusion tensor imaging. Magn Reson Imaging 2001;19:937–950.
16. Zhuang J, Hrabe J, Kangarlu A, et al. Correction of eddy current distortions in diffusion tensor imaging using the known gradient strengths and directions. J Magn Reson Imaging 2006;24:1188–1193.
17. Anderson E, Bai Z, Bischof C, et al. LAPACK users' guide, 3rd ed. Philadelphia: Society for Industrial and Applied Mathematics; 1999.
18. Wang R, Benner T, Sorensen AG, Wedeen VJ. Diffusion toolkit: a software package for diffusion imaging data processing and tractography. Proc. In: Proc 15th Annual Meeting ISMRM, Berlin; 2007. p 3720.
19. Mori S, Crain BJ, Chacko VP, van Zijl PCM. Three dimensional tracking of axonal projections in the brain by magnetic resonance imaging. Ann Neurol 1999;45:265–269.
20. Andersson JLR, Skare S. A model-based method for retrospective correction of geometric distortions in diffusion-weighted EPI. NeuroImage 2002;16:177–199.